

## High-sensitivity, high-selectivity detection of chemical warfare agents

Michael B. Pushkarsky, Michael E. Webber,<sup>a)</sup> and Tyson Macdonald  
Pranalytica, Inc., 1101 Colorado Avenue, Santa Monica, California 90401

C. Kumar N. Patel<sup>b)</sup>  
Pranalytica Inc., 1101 Colorado Avenue, Santa Monica, California 90401  
and Department of Physics & Astronomy, University of California, Los Angeles, California 90095

(Received 16 May 2005; accepted 30 November 2005; published online 27 January 2006)

We report high-sensitivity detection of chemical warfare agents (nerve gases) with very low probability of false positives (PFP). We demonstrate a detection threshold of 1.2 ppb ( $7.7 \mu\text{g}/\text{m}^3$  equivalent of Sarin) with a PFP of  $<1:10^6$  in the presence of many interfering gases present in an urban environment through the detection of diisopropyl methylphosphonate, an accepted relatively harmless surrogate for the nerve agents. For the current measurement time of  $\sim 60$  s, a PFP of  $1:10^6$  corresponds to one false alarm approximately every 23 months. The demonstrated performance satisfies most current homeland and military security requirements. © 2006 American Institute of Physics. [DOI: 10.1063/1.2166692]

Optical spectroscopy has long been used for identifying chemical compounds and is a relevant technique because the CWAs have strong optical absorption features in the infrared in the 9–11.5  $\mu\text{m}$  region (Fig. 1, top panel), with absorption strengths<sup>1</sup> of  $(1-6) \times 10^{-3}$  (ppm meter)<sup>-1</sup>. Detection of these gases at ppb levels of interest will necessitate absorption coefficient measurements of  $(1-6) \times 10^{-8} \text{ cm}^{-1}$ . Laser photoacoustic spectroscopy (L-PAS) permits such measurements in short optical pathlengths.<sup>2-4</sup> Because high-power ( $>1$  W)  $\text{CO}_2$  lasers are available with wide tunability (Fig. 1, bottom panel) throughout the 9–11.5  $\mu\text{m}$  where the CWAs absorb, they are ideal laser sources for L-PAS systems for the detection of the CWAs.

For the detection the CWAs in real environments, however, high sensitivity alone is not sufficient. Sensor must have very few false alarms to avoid unacceptable social and economic disruptions. The problem of interference rejection is severe because the broad absorption features of many interferences<sup>5</sup> overlap with the broad absorption features of the target CWA. In normal indoor or outdoor environments, hundreds of gases are present, of which a few dozen need special consideration because of their ambient concentrations, absorption magnitudes, and spectral overlap with the CWAs. A simulation model has shown<sup>5</sup> that L-PAS in this wavelength region could detect the CWAs at very low concentrations with very low PFP by using multiple wavelengths of the  $\text{CO}_2$  laser to map the spectral signature of the target gas in a “soup” of background species.

Principles of L-PAS have been described in many papers. Our photoacoustic spectrometer<sup>6</sup> includes a  $^{13}\text{CO}_2$  laser that is tuned across 34 laser transitions in the P and R branches of the  $00^0_1-[10^0_0, 02^0_0]_{||}$  band, covering 9.6 to 10.2  $\mu\text{m}$  in  $\sim 40$  seconds. The normalized PA on a laser transition is proportional to the cumulative optical absorption caused by all of the gases present in the cell including CWAs. The individual contribution from CWAs and the

other species is extracted using the spectral libraries recorded with the spectrometer and a linear pattern recognition<sup>5</sup> algorithm embedded in the analyzer. Diisopropyl methylphosphate (DIMP), an accepted and a relatively harmless surrogate for CWAs, was used to demonstrate the performance of the L-PAS for CWA detection.

Figure 2 shows the spectral libraries used to evaluate  $\alpha_{i,\lambda_j}$ , the absorption coefficient of species  $i$  at wavelength  $\lambda_j$ . Three additional vectors were added to account for the offset, slope, and curve of the background signals. When a mixture of trace gases is present in the photoacoustic cell, the total absorption  $\alpha_{\lambda_j}$  at a specific wavelength  $\lambda_j$  is given by

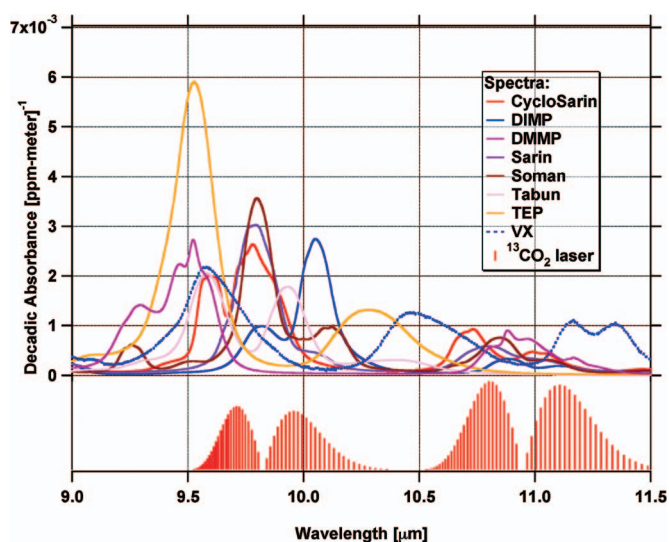


FIG. 1. (Color) Spectral absorption features of Tabun (GA), Sarin (GB), Soman (GD), Cyclosarin (GF), VX, triethyl phosphate (TEP), dimethyl methylphosphonate (DMMP), and diisopropyl methylphosphonate (DIMP) in the 9–11.5  $\mu\text{m}$  region (top panel); positions and relative power levels of the  $^{13}\text{CO}_2$  laser output on the lasing transitions as a function of the wavelength (bottom panel). The left group of transitions corresponding to the P and R branches of the  $00^0_1-[10^0_0, 02^0_0]_{||}$  band are used in the present studies to evaluate the performance of the L-PAS spectrometer for the detection of CWAs.

<sup>a)</sup>Present address: Rand Corporation, 1776 Main Street, P.O. Box 2138, Santa Monica, CA 90407.

<sup>b)</sup>Author to whom correspondence should be addressed; electronic mail: patel@pranalytica.com

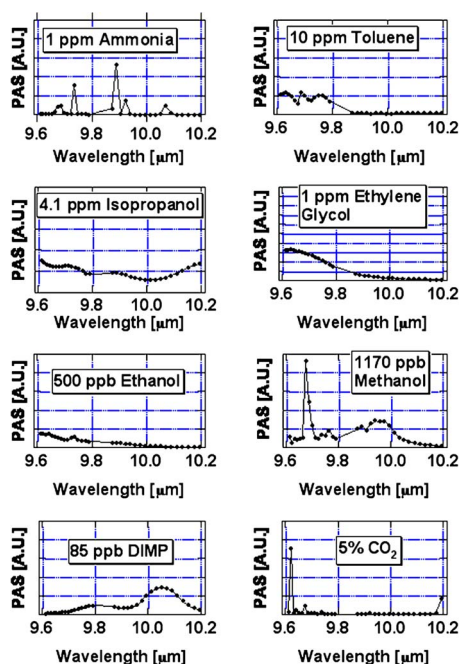


FIG. 2. Measured photoacoustic absorption spectra for ammonia, toluene, isopropanol, ethylene glycol, ethanol, methanol, DIMP, and CO<sub>2</sub>. Dots represent measured PAS signals at the peak of the <sup>13</sup>CO<sub>2</sub> laser lines.

$$\begin{aligned} \text{Absorption Coefficient}_{\lambda_j} &= \alpha_{\lambda_j} = \sum_{i=1}^{\text{\# of species}} \alpha_{i,\lambda_j} \\ &= \sum_{i=1}^{\text{\# of species}} \sigma_{i,\lambda_j} X_i, \end{aligned} \quad (1)$$

where  $\sigma_{i,\lambda_j}$  is the absorbance for species  $i$  at wavelength  $\lambda_j$ , and  $X_i$  is the mole fraction of the species  $i$ . The measured signal is linear for over five orders of magnitude until the cumulative optical density approaches 6% or greater.<sup>7</sup> Finally, from the measured absorption strength matrix  $\alpha_{i,\lambda_j}$ , we derive concentration of the specific component.<sup>5</sup>

L-PAS analyzer performance to measure DIMP was evaluated in the presence of eight species listed in Table I that were determined in the simulations to be the worst expected interferents.<sup>5</sup> Analyzer performance is a combination

TABLE I. Components and concentrations used in the present study for synthetic clean air, outdoor Santa Monica air, and synthetic contaminated air.

Component	Concentrations for synthetic clean air	Concentrations for Santa Monica air	Concentrations for synthetic contaminated air
Nitrogen	79%	79%	79%
Oxygen	20%	20%	20%
Water	1%	1%–2%	1%
Carbon dioxide	500 ppm	300–550 ppm	500 ppm
n-propanol	None	Unknown	730 ppb
Ethylene Glycol	None	Unknown	360 ppb
Toluene	None	Unknown	3.6 ppm
Methanol	None	Unknown	830 ppb
Ammonia	None	Unknown	700 ppb
Ethanol	None	Unknown	330 ppb
All others	None	Unknown	None

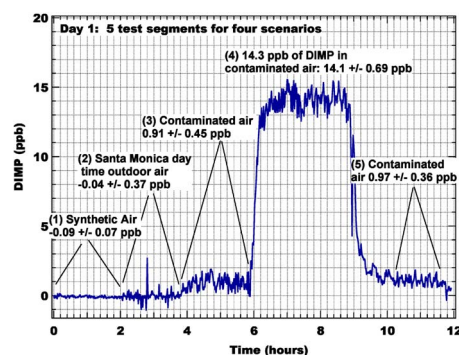


FIG. 3. L-PAS analyzer measurements of DIMP in 5 segments: (1) synthetic clean air, (2) Santa Monica city street air, (3) synthetic contaminated air with no DIMP, (4) synthetic contaminated air with 14.3 ppb DIMP present, and (5) synthetic contaminated air with no DIMP.

of sensitivity, accuracy, and selectivity (low false alarms when the target gas is not present). Four different measurement scenarios were used:

- (1) 0 ppb DIMP in synthetic clean air to determine best-case sensitivity,
- (2) 0 ppb DIMP in real outdoor Santa Monica air to establish a benchmark for sensitivity and selectivity in nominal urban conditions,
- (3) 0 ppb DIMP in synthetic, highly contaminated air to establish sensitivity and selectivity under extreme conditions,
- (4) 14.3 ppb DIMP in synthetic contaminated air to establish accuracy.

The results of these four test cases are plotted in Fig. 3 with five different test segments (case 3 is conducted twice), and summarized in Table II. Case 1 is used to establish a benchmark for sensitivity with synthetic clean air (O<sub>2</sub>, N<sub>2</sub>, 1% H<sub>2</sub>O, 500 ppm CO<sub>2</sub>) and no DIMP present; the analyzer produced an average DIMP reading of  $-0.09 \pm 0.07$  ppb (1 $\sigma$ ) over 120 successive measurements (Fig. 3, segment 1). Thus, the best-case sensitivity for the system is approximately 70 ppt ( $0.51 \mu\text{g}/\text{m}^3$ ) and the zero-level is within 100 ppt of true zero.

Testing the L-PAS under nominal urban contamination levels was achieved in case 2 by measuring daytime outdoor Santa Monica air with no DIMP present (see Table I). For this test (Fig. 3, segment 2) 110 successive measurements yielded an average DIMP reading of  $-0.04 \pm 0.37$  ppb corresponding to a sensitivity of  $2.7 \mu\text{g}/\text{m}^3$ . The cumulative effect of the interferences is a degradation of the sensitivity by a factor of  $\sim 6$ , but with no effect on the zero level, which remained within 100 ppt of true zero.

TABLE II. Measurement results for each test segment.

Segment	Test Conditions	Actual DIMP concentration	Measured DIMP concentration
①	Synthetic clean air	0 ppb	$-0.09 \pm 0.07$ ppb
②	Santa Monica outdoor air (daytime)	0 ppb	$-0.04 \pm 0.37$ ppb
③	Synthetic contaminated air	0 ppb	$0.91 \pm 0.45$ ppb
④	Synthetic contaminated air	14.3 ppb	$14.1 \pm 0.69$ ppb
⑤	Synthetic contaminated air	0 ppb	$0.97 \pm 0.36$ ppb

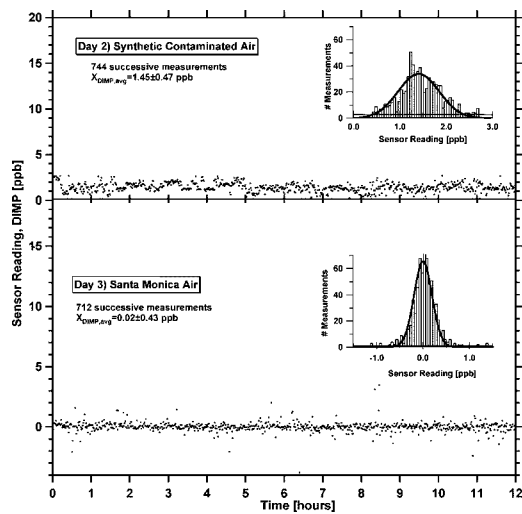


FIG. 4. Measurements of DIMP in synthetic contaminated air and Santa Monica air over 12 h on different days to determine the sensitivity and PFP. Histograms for both days are shown as insets, with Gaussian curve fits used to estimate PFP. For example, for the situation represented in the top panel for highly contaminated synthetic ambient air, PFP for a detection (alarm) threshold of 2 ppb is calculated by taking the ratio of the area under the histogram for sensor reading  $>2$  ppb and the total area under the histogram. For a 2 ppb alarm threshold, this situation yields an unacceptable level of PFP of about 10%. Increasing the threshold to 3.5 ppb lowers the PFP to an acceptable  $10^{-6}$ .

A performance test in highly contaminated conditions was conducted by analyzing a synthetic air mixture shown in Table I, the components of which are expected to be significant interferences.<sup>5</sup> The concentration for each species was picked to be at levels exceeding those expected to be found in indoor contaminated air to serve as a strict test. The results, shown in the segments 3 and 5 (Fig. 3) reveal that the interferences cause the zero-level increase to an average reading of 0.91 and 0.97 ppb DIMP for the two respective segments, and degrade the  $1\sigma$  precision to 0.45 and 0.36 ppb ( $3.3$  and  $2.7 \mu\text{g}/\text{m}^3$ ), respectively. For reference, a typical CWA (Sarin) exposure that causes the first noticeable health effect (miosis<sup>8</sup>) is  $1 \text{ mg}\cdot\text{min}/\text{m}^3$ ; that is, a permissible concentration<sup>9-11</sup> of about  $33 \mu\text{g}/\text{m}^3$  ( $5.8$  ppb) for an exposure of 30 min, and  $16 \mu\text{g}/\text{m}^3$  ( $2.9$  ppb) for an exposure of 60 min. The L-PAS accuracy in the presence of interferences

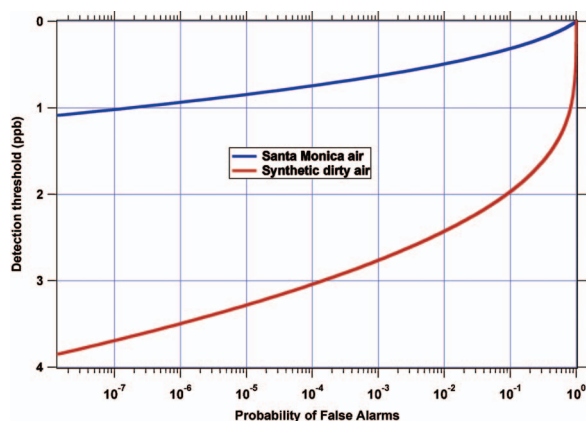


FIG. 5. (Color) Measured receiver operation characteristic curve for the detection of DIMP, an accepted surrogate for Sarin, in the presence of Santa Monica street air and synthetic dirty air.

was established by adding  $14.3$  ppb DIMP to the synthetic contaminated air mixture. The L-PAS gave an average reading of  $14.1 \pm 0.69$  ppb (Fig. 3, segment 4), yielding excellent accuracy and a precision.

The experimental data for apparent DIMP values when it is not present permit us to estimate PFP for a particular alarm threshold. The PFP is the number of times the sensor indicates that DIMP is present above the alarm threshold even when no DIMP is present. The PFP is evaluated using the statistical noise characteristics of the observed “zero DIMP” signal.<sup>5</sup> The statistical variation of sensor readings over 12 h of measurements for the cases 2 and 3 are shown in Fig. 4. The average of sensor readings for synthetic contaminated air over the 12 h period on day 2 and for Santa Monica outdoor air over the 12 h period on day 3 were  $1.45 \pm 0.47$  ppb (the offset is the result of interferences, rather than from residual DIMP) and  $0.02 \pm 0.43$  ppb, respectively.

Histograms for each of the two cases, with  $>700$  data points, are shown as insets. The PFP is calculated by performing a Gaussian fit to the histograms and then comparing the area under the curve above the alarm level with the total area under the curve. Figure 5 shows a plot of alarm threshold versus PFP (receiver operation characteristic, ROC) evaluated from the data in Fig. 4. For synthetic contaminated air, a false alarm will occur once every million measurements for an alarm threshold of  $3.5$  ppb ( $20 \mu\text{g}/\text{m}^3$  equivalent of Sarin), while for Santa Monica outdoor air the results are much better, and a PFP of  $1:10^6$  is achieved with a lower threshold of  $0.95$  ppb ( $6.1 \mu\text{g}/\text{m}^3$  equivalent of Sarin). A PFP of  $1:10^6$  leads to one false alarm every  $\sim 23$  months (measurement time of 1 min). Both alarm settings are lower than the 30 min exposure threshold for miosis ( $33 \mu\text{g}/\text{m}^3$  or  $5.8$  ppb), and are satisfactory for the 60 min threshold ( $16 \mu\text{g}/\text{m}^3$  or  $2.9$  ppb) and should be adequate for warning the population at large about a CWA attack. It should be noted that the ROC curves (Fig. 5) permit a user to optimize the alarm threshold and the PFP depending on specific applications.

This work was supported, in part, through a DARPA contract MDA972-02-C-0092 (Approved for Public Release, Distribution Unlimited).

<sup>1</sup>S. W. Sharpe, R. L. Sams, T. J. Johnson, P. M. Chu, G. C. Rhoderick, and F. R. Guenther, Proc. SPIE **4577**, 12 (2001).

<sup>2</sup>L. B. Kreuzer, J. Appl. Phys. **42**, 2934 (1971).

<sup>3</sup>*Topics in Current Physics: Photoacoustic, Photothermal and Photochemical Processes in Gases*, edited by P. Hess (Springer, Berlin, 1989).

<sup>4</sup>M. B. Pushkarsky, M. E. Webber, and C. K. N. Patel, Appl. Phys. B: Lasers Opt. **77**, 381 (2003).

<sup>5</sup>M. E. Webber, M. B. Pushkarsky, and C. K. N. Patel, J. Appl. Phys. **97**, 113101 (2005).

<sup>6</sup>M. B. Pushkarsky, M. E. Webber, T. N. Macdonald, and C. K. N. Patel (unpublished).

<sup>7</sup>A. Schmohl, A. Miklos, and P. Hess, Appl. Opt. **41**, 1815 (2002).

<sup>8</sup>The first noticeable health effect is miosis, which for Sarin includes pin-pointing of the pupil of the eye accompanied by runny nose, tightness of the chest, and eye pain.

<sup>9</sup>Department of the Army, *Army Field Manual No. 3-9; Potential Military Chemical/Biological Agents and Compounds* (Headquarters of the Army, Washington, D.C., 1990), pp. 19–20.

<sup>10</sup>B. McNamara and L. Leitmaker, *Edgewood Arsenal Special Publication* (U.S. Army, Medical Research Laboratories, Edgewood Arsenal, Aberdeen Proving Grounds, MD, 1971).

<sup>11</sup>Department of Health and Human Services, Center for Disease Control, Federal Register **53**, 8504 (1988).